Supplementary Information

Nickel(II) porphyrin/fullerene C_{70} porous molecular cocrystal featuring a robust one-dimensional channel

Nobuhiro Sato,[a] Kosuke Toki,[a] Tomoki Tateishi,[a,b] Masaya Tsumura,[c] Ryojun Toyoda,[a] Shinya Takaishi,[a] Yuki Kurashige,[b] Kunihisa Sugimoto,[d] and Ryota Sakamoto*[a,e]

a. Department of Chemistry, Graduate School of Science, Tohoku University, 6-3 Aramaki Aza-Aoba, Aoba-ku, Sendai 980-8578, Japan.

b. Frontier Research Institute for Interdisciplinary Sciences (FRIS), Tohoku University Aramaki aza Aoba 6-3, Aoba-ku, Sendai 980-8578, Japan.

c. Department of Chemistry, Graduate School of Science, Kyoto University, Kitashirakawa Oiwake-cho, Sakyo-ku, Kyoto, Japan.

d. Department of Chemistry, Kindai University, 3-4-1 Kowakae, Higashi-Osaka, Osaka 577-8502, Japan.

e. Division for the Establishment of Frontier Sciences of Organization for Advanced Studies at Tohoku University, 2-1-1 Katahira, Aoba-ku, Sendai 980-8577, Japan.

Materials, characterization and calculation methods

All chemicals were purchased from commercial suppliers, and they were used without further purification unless otherwise noted. The diffraction data for all crystals were mounted on a cryoloop and placed in the nitrogen stream (T = 120 or 300 K) and collected on a Rigaku XtaLAB AFC10 diffractometer with a HyPix-6000HE hybrid pixel array detector, graphite monochromated Mo Kα radiation (λ = 0.7107 Å) and a cryogenic equipment GN-2D/S. The crystal structures were solved using direct methods (SHELXT) followed by Fourier synthesis. Structure refinement was performed using full matrix least-squares procedures with SHELXL on F2 in the Olex2 software. CCDC 2527177 - 2527179 contain the supplementary crystallographic data for this paper. These data can be obtained free of charge via www.ccdc.cam.ac.uk/data_request/cif. Void calculation was performed using Mercury software. The hydrogen atoms were generated by geometrical considerations, constrained by idealized geometries and allowed to ride on their carrier atoms with an isotropic displacement parameter related to the equivalent displacement parameter of their carrier atoms. The high-pressure single crystal diffraction data experiments were conducted at 300 K with radiation wavelength of λ = 0.4135 Å, at SPring-8, BL02B1 beamline. A single crystal of the sample and small amount of ruby powder was placed in a Diamond Anvil Cell (DAC) with Fluorinert 43 as the pressure transmitting medium. The pressure inside the DAC chamber was determined using the ruby fluorescence method. The diffraction frames were collected on a Pilatus 1M CdTe detector. Lattice parameters were obtained with CrysalisPro software.[1] UV–vis–NIR diffuse reflectance spectra were collected on a Shimadzu UV-3100PC spectrometer attached with a Shimadzu ISR-3100 integrating sphere. For solid-state UV, $BaSO_4$ was used as a nonabsorbing matrix to dilute the sample. Obtained diffuse reflectance spectra were converted into absorption spectra by applying the Kubelka–Munk function $F(R) = (1 - R)^2/2R$. Gas sorption measurement was performed by Belsorp-max. N_2 sorption data was analyzed using BELmasterTM. Powder X-ray diffraction (PXRD) patterns were collected on a Rigaku Smartlab© with Cu Ka radiation (λ = 1.5406 Å) at room temperature. FT-IR spectra were acquired using a Jasco FT/IR-4200 spectrometer. Therein, an attenuated total refraction (ATR) attachment with a ZnSe window was used. The structures of porphyrin-fullerene cocrystals (**NiTEPP/C_{60}**, three types of disordered **NiTEPP/C_{70}**, and **NiTEPP/C_{70}-n**) were optimized using the Gaussian Plane Wave (GPW) method[2] implemented in CP2K program.[3] Initially, a unit cell containing four fullerenes was constructed from the crystal structure at 120 K, and the geometry and lattice constants optimization was performed. To evaluate the intermolecular interaction energy, the **NiTEPP** framework and the single fullerene molecule were extracted from the optimized unit cell, and their energies were calculated separately. The interaction energy ΔE was defined as follows:

$$\Delta E = E(\text{cocrystal}) - E(\text{NiTEPP framework}) - 4 \times E(\text{fullerene molecule})$$

The Perdew-Burke-Ernzerhof (PBE) functional[4], the DZVP-MOLOPT-SR-GTH basis set[5], and GTH-PBE pseudopotentials[6] were employed with DFT-D3(BJ) dispersion correction[7] to account for van der

Waals interaction. The planewave cutoff energy was set to 320 Ry with a relative cutoff 30 Ry. The k-point mesh was set to $1 \times 1 \times 1$, or Γ point only. The optimization was terminated when the maximum and the root mean square of the force got lower than 1.0×10^{-3} a.u.

Single-crystal preparation for NiTEPP/C_{70}, NiTEPP/C_{70}-n

NiTEPP was synthesized according to a previously reported procedure[8–10]. NiTEPP (1.7 mg, 2.2 mmol) and C_{70} (1.2 mg, 1.8 mmol) were dissolved in 2.0 mL of a $CHCl_3$ / CS_2 mixed solvent (1:1, v/v). The resulting solution was placed in a vial, which was then set inside a larger vial containing hexane as poor solvent, with the liquid levels of the inner and outer vials adjusted to be the same (**Figure S1**). After 1–2 weeks, the resulting crystals were collected by filtration.

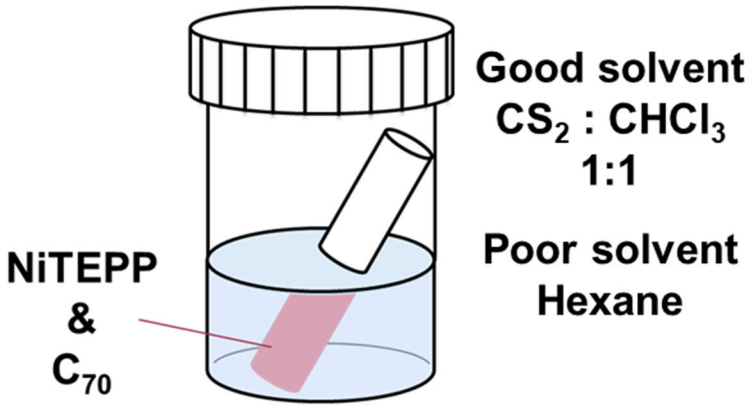

Fig. S1. Schematic illustration of the synthesis of **NiTEPP/C_{70}** and **NiTEPP/C_{70}-n**.

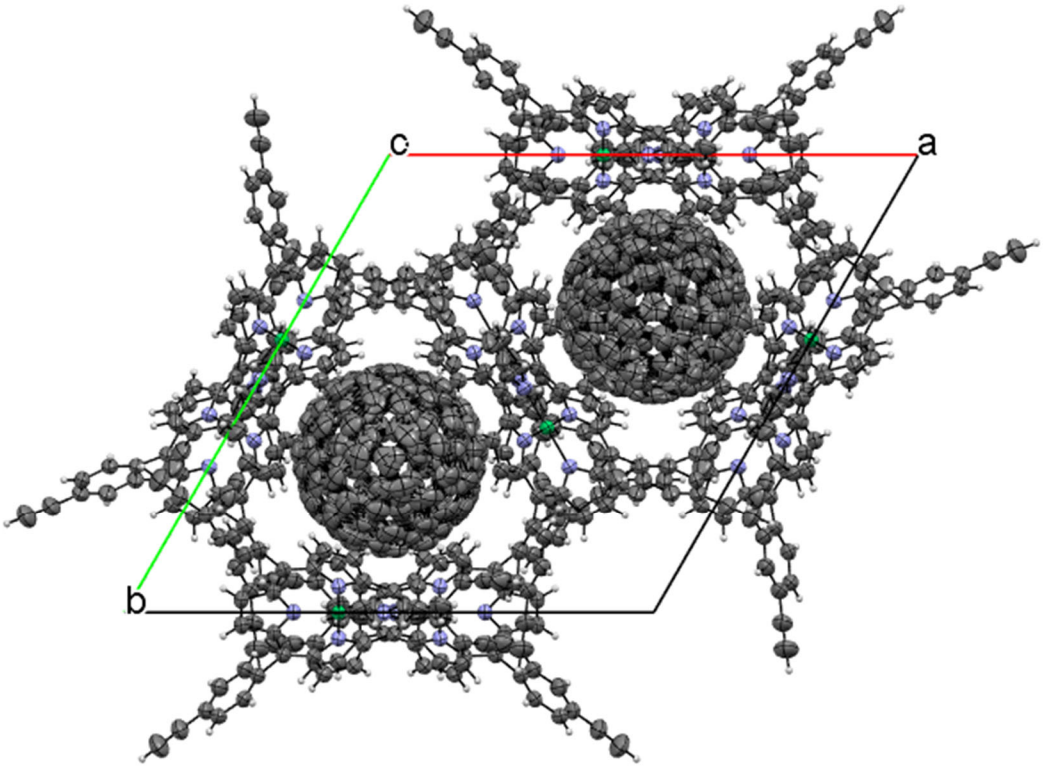

Fig. S2. Unit cell of **NiTEPP/C_{70}** viewed along the *c* axis.

Table S1. Crystallographic data for **NiTEPP/C_{70}** collected at 120 K

Identification code	NiTEPP/C_{70}
Empirical formula	$C_{98.67}H_{28}N_4Ni$
Formula weight	1327.96
Temperature/ K	120
Crystal system	trigonal
Space group	$P\bar{3}c1$
a / Å	22.4788(6)
b / Å	22.4788(6)
c / Å	22.3082(10)
α / °	90
β / °	90
γ / °	120
Volume / $Å^3$	9762.1(7)
Z	6
ρ_{calc} g/cm^3	1.355
μ / mm^{-1}	0.357
F(000)	4056.0
Crystal size / mm^3	0.35 × 0.2 × 0.18
Radiation	Mo Kα (λ = 0.71073)
2Θ range for data collection / °	5.146 to 67.502
Index ranges	$-34 \le h \le 29$, $-28 \le k \le 34$, $-34 \le l \le 34$
Reflections collected	136768
Independent reflections	12185 [R_{int} = 0.0871, R_{sigma} = 0.0525]
Data/restraints/parameters	12185/0/473
Goodness-of-fit on F^2	1.022
Final R indexes [$I \geqq 2\sigma(I)$]	R_1 = 0.1204, wR_2 = 0.2779
Final R indexes [all data]	R_1 = 0.2050, wR_2 = 0.3250
Largest diff. peak/hole / e $Å^{-3}$	0.85/-0.63

Disorder treatment of the C_{70} unit in NiTEPP/C_{70}

The space group of **NiTEPP/C_{70}** is $P\bar{3}c1$. Unlike C_{60}, the C_{70} molecule does not possess threefold rotational symmetry, and therefore a fully ordered C_{70} molecule cannot be placed on a crystallographic threefold axis without introducing inconsistencies in the structural model. Since the crystal structure is generated by applying symmetry operations to the asymmetric unit, the presence of a molecule lacking the corresponding symmetry inevitably results in orientational disorder.

Accordingly, the C_{70} molecule was modeled as a symmetry-related disorder with an occupancy of 1/3 in the asymmetric unit. In this model, three equivalent orientations generated by the crystallographic threefold axis collectively correspond to one C_{70} molecule.

During refinement using Olex2, a C_{70} fragment was selected from the Fragment Database and positioned to match the Q peaks attributed to C_{70}, as shown in **Figure S3**. The chemical occupancy was fixed at 1/3, and the PART instruction was set to –1. Upon refinement, three symmetry-related C_{70} orientations were generated, resulting in an overall occupancy equivalent to one C_{70} molecule.

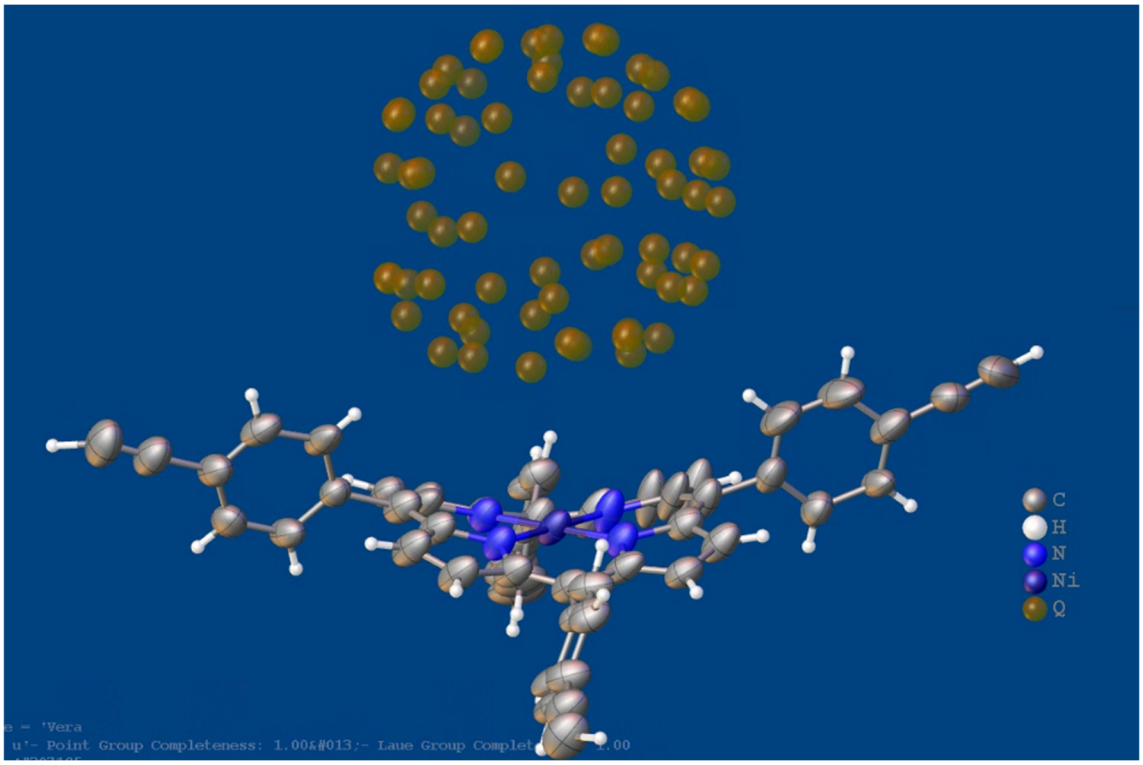

Fig. S3. Screenshot of the Olex2 interface during the structure refinement of **NiTEPP/C_{70}**.

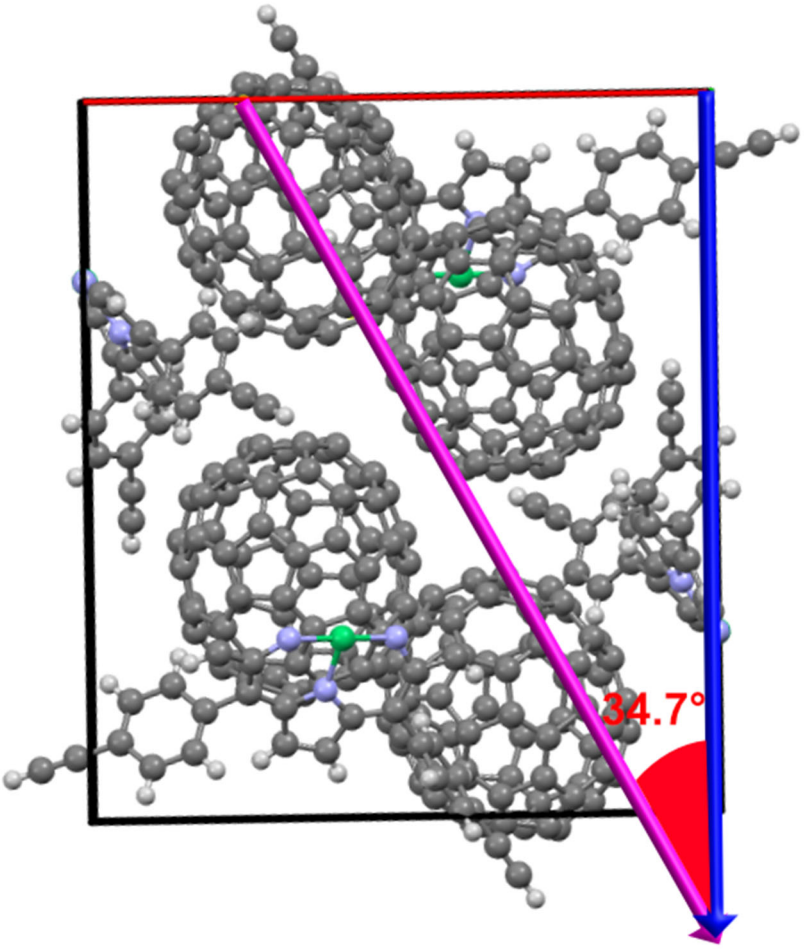

Fig. S4. Illustration showing the orientation of the fullerene molecules in **NiTEPP/C_{70}**. Some atoms are omitted for clarity. The pink arrows indicate the long axis of C_{70}, while the blue arrows represent the crystallographic *c* axis.

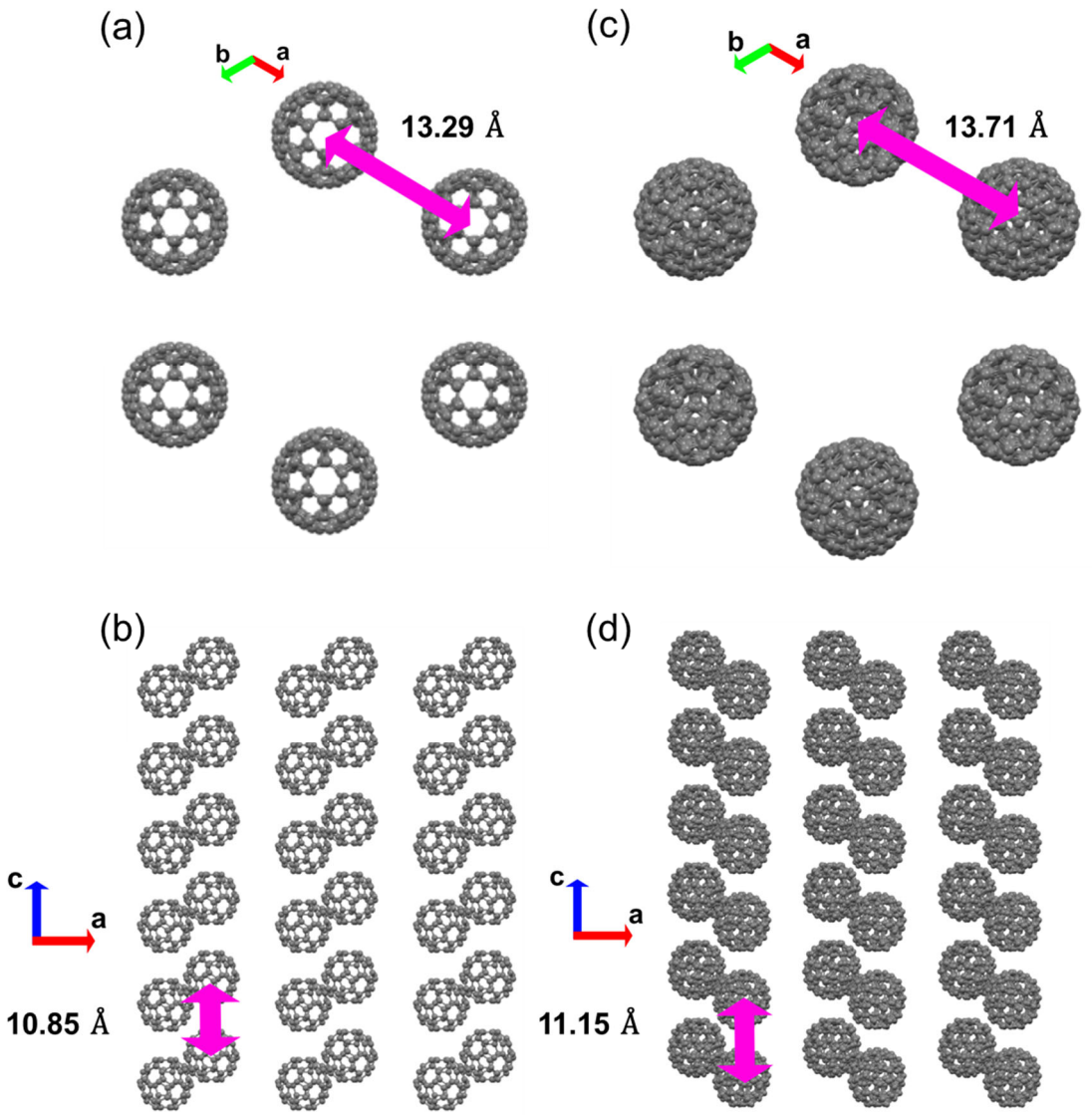

Fig. S5. Distances between the centroids of neighboring fullerene molecules the *a*,*b* network directions and *c* axis direction. Porphyrin molecules are omitted for clarity. (a). Crystal structure of **NiTEPP/C_{60}** viewed along the *c* axis. (b). Crystal structure of **NiTEPP/C_{60}** viewed along the *b* axis. (c) Crystal structure of **NiTEPP/C_{70}** viewed along the *c* axis. (d) Crystal structure of **NiTEPP/C_{70}** viewed along the *b* axis.

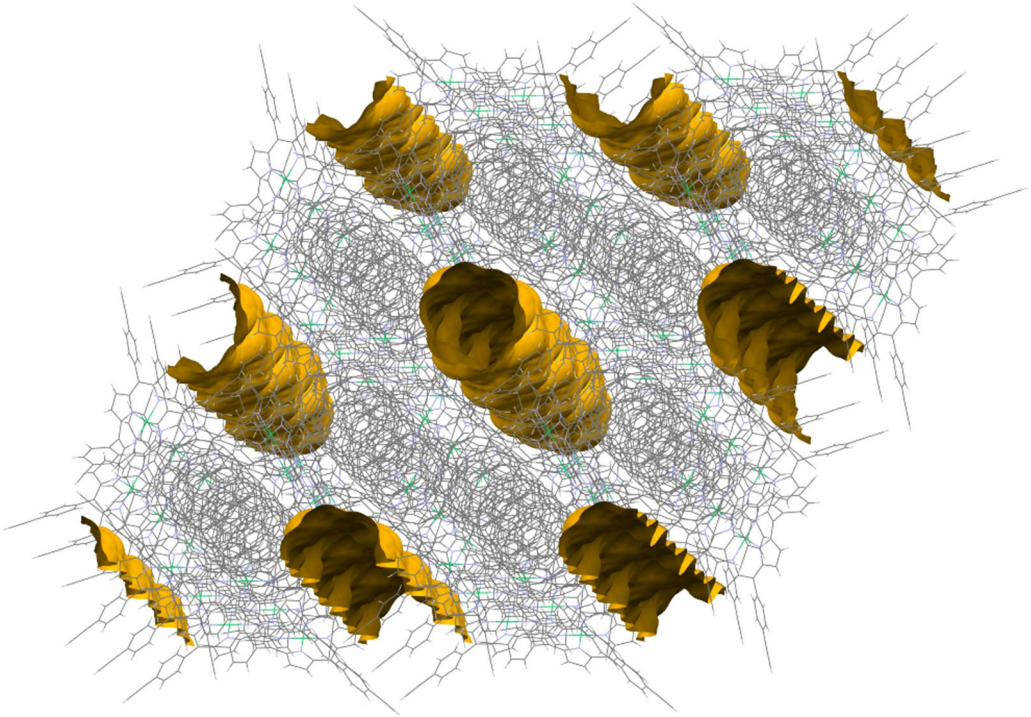

Fig. S6. Void representation of **NiTEPP/C_{60}**, generated using the void calculation function implemented in the Mercury software. Atom colors: Ni (yellow green), N (light blue), C (gray), and H (white).

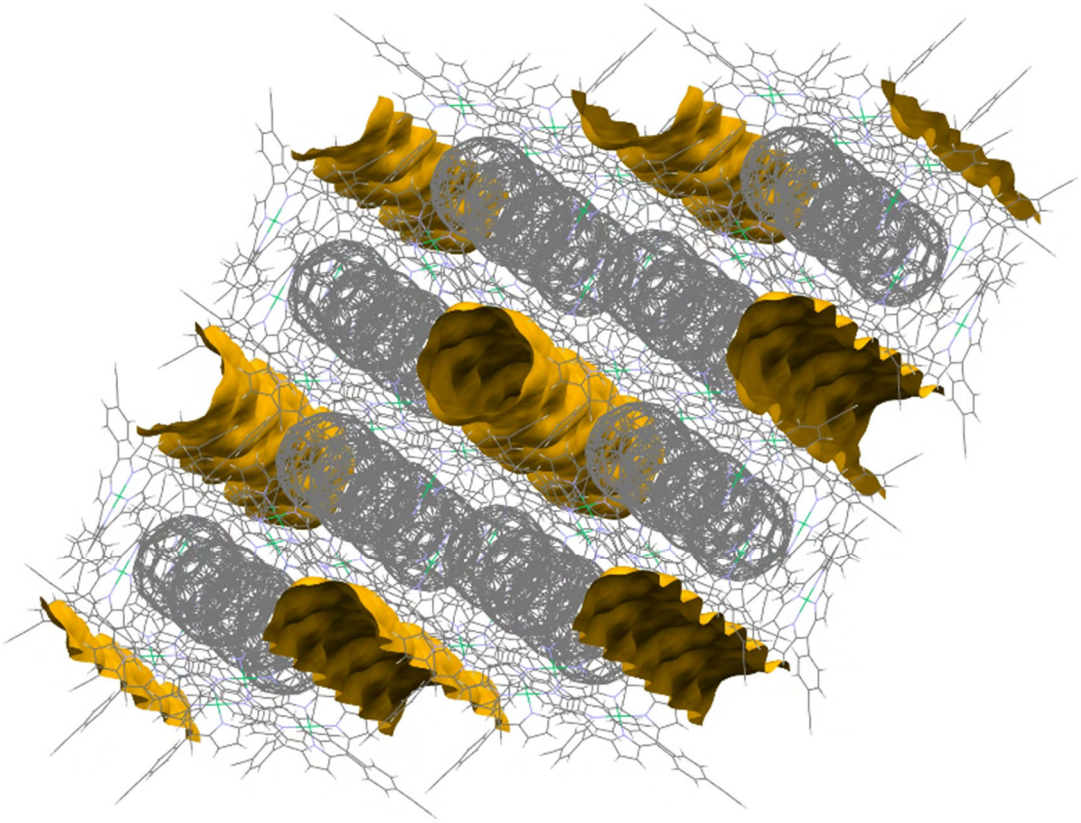

Fig. S7. Void representation of **NiTEPP/C_{70}**, generated using the void calculation function implemented in the Mercury software. Atom colors: Ni (yellow green), N (light blue), C (gray), and H (white).

Calculation of the void radius of NiTEPP/C_{70}

The crystal structures were visualized using Mercury software. When viewed along the c axis in the space-filling representation, the centroid of the three hydrogen atoms (highlighted in yellow) that are most exposed toward the void was identified (**Figure S9**). Owing to crystallographic symmetry, these three hydrogen atoms lie on the same plane, and accordingly, their centroid is also located on this plane. The distance from this centroid to each hydrogen atom was measured (**Figure S10**), and the smallest of these distances was taken as the minimum radius from the center of the void to the surrounding atoms. From the measured value, the van der Waals radius of hydrogen (0.60 Å) was subtracted to obtain the effective void radius.[2] The same procedure was applied to **NiTEPP/C_{70}**.

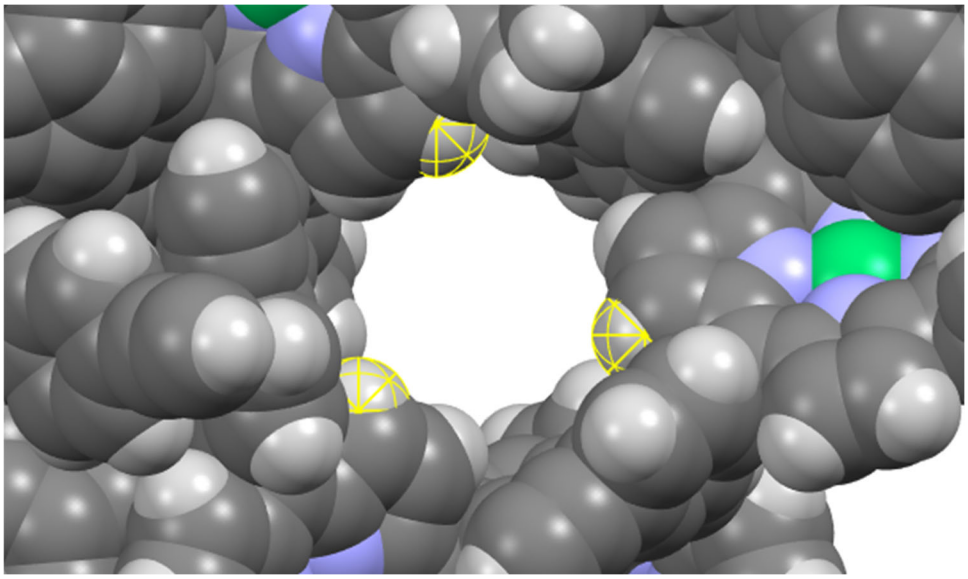

Fig. S8. Space-filling representation of NiTEPP/C_{60} at 120 K. Atom colors: Ni (yellow green), N (light blue), C (gray), and H (white).

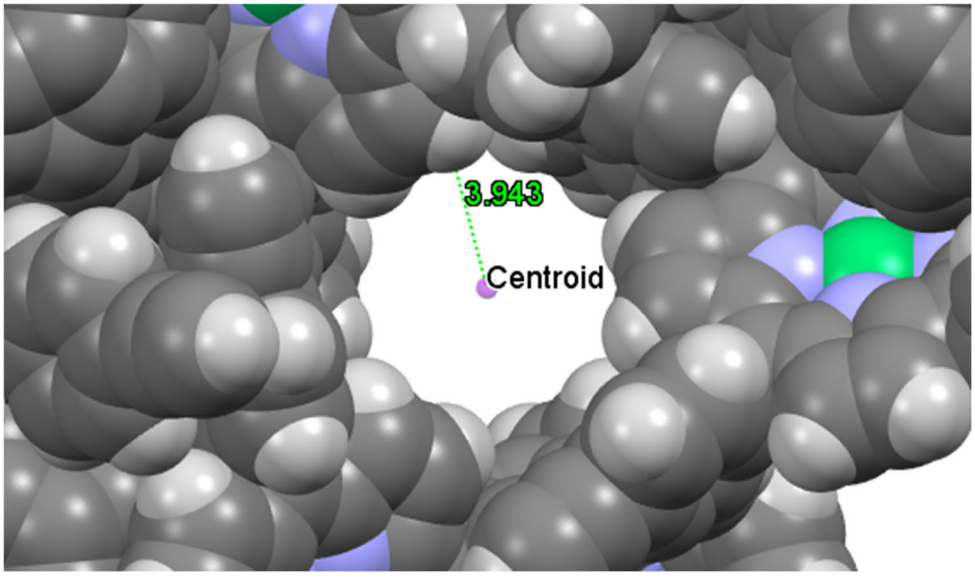

Fig. S9. Space-filling representation of **NiTEPP/C_{60}** at 120 K, highlighting the centroid of the hydrogen atoms selected in Figure S9. Atom colors: Ni (yellow green), N (light blue), C (gray), and H (white).

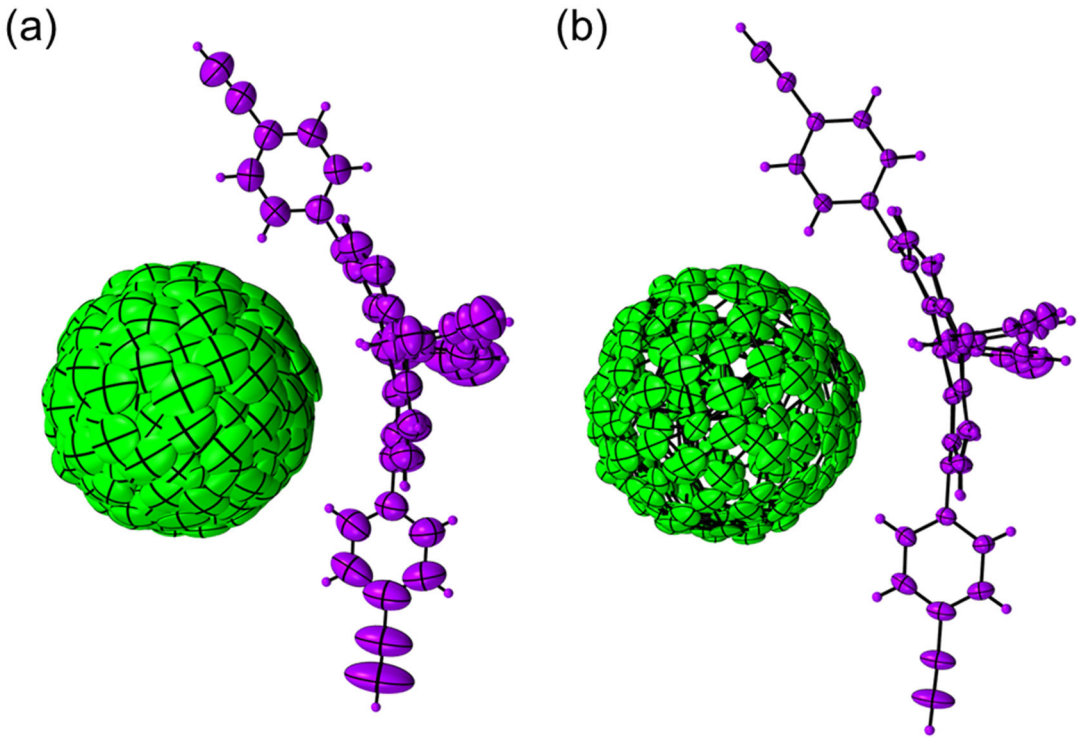

Fig. S10. ORTEP drawing of **NiTEPP/C_{70}** at 293 K. (a) Thermal ellipsoids are drawn at the 50% probability level. The carbon atoms of the C_{70} molecules exhibit severe disorder, effectively enveloping the outer region. (b) Thermal ellipsoids are drawn at the 15% probability level. **NiTEPP** molecules are shown in purple, and C_{70} molecules in green.

Table S2. Crystallographic data for **NiTEPP/C_{70}** collected at 293 K

Identification code	NiTEPP/C_{70}
Empirical formula	$C_{98.67}H_{28}N_4Ni$
Formula weight	1327.96
Temperature/ K	293
Crystal system	trigonal
Space group	$P\bar{3}c1$
a / Å	23.0532(7)
b / Å	23.0532(7)
c / Å	21.9053(7)
α / °	90
β / °	90
γ / °	120
Volume / Å^3	10081.9(7)
Z	6
ρ_{calc} g/cm^3	1.312
μ / mm^{-1}	0.345
F(000)	4056.0
Crystal size / mm^3	0.14 × 0.13 × 0.12
Radiation	Mo Kα (λ = 0.71073)
2Θ range for data collection / °	5.130 to 67.396
Index ranges	$-32 \le h \le 34$, $-34 \le k \le 33$, $-25 \le l \le 33$
Reflections collected	128932
Independent reflections	11990 [R_{int} = 0.0755, R_{sigma} = 0.1070]
Data/restraints/parameters	11990/7523/892
Goodness-of-fit on F^2	1.005
Final R indexes [$I \geqq 2\sigma(I)$]	R_1 = 0.0838, wR_2 = 0.1675
Final R indexes [all data]	R_1 = 0.1678, wR_2 = 0.2175
Largest diff. peak/hole / e Å^{-3}	0.22/-0.35

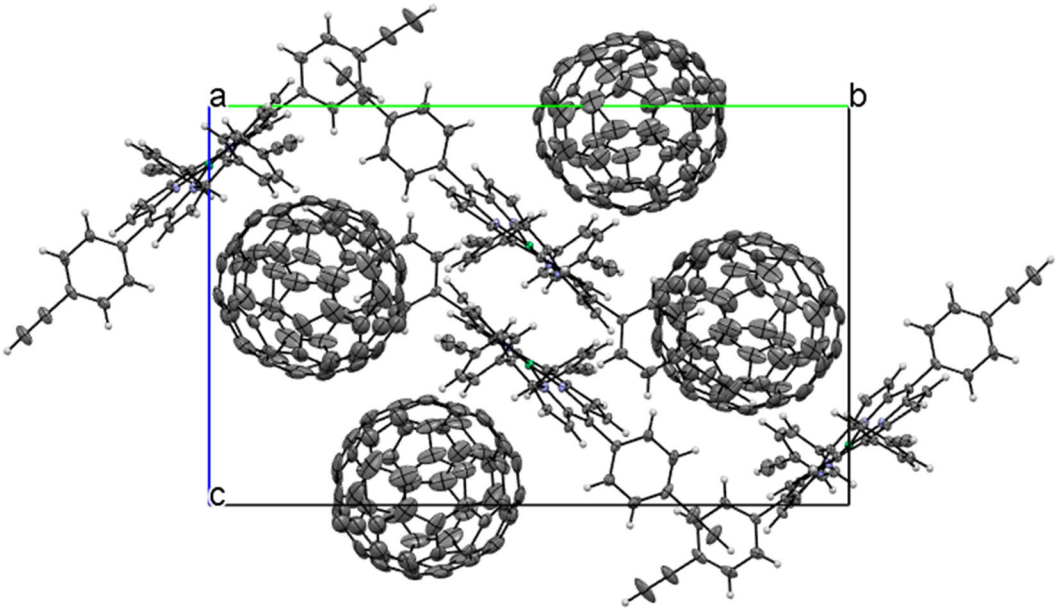

Fig. S11. Unit cell of **NiTEPP/C_{70}-n** viewed along the *a* axis.

Table S3. Crystallographic data for **NiTEPP/C_{70}-n** collected at 120 K

Identification code	NiTEPP/C_{70}-n
Empirical formula	$C_{122}H_{28}N_4Ni$
Formula weight	1608.19
Temperature/ K	120
Crystal system	monoclinic
Space group	$P2_1/n$
a / Å	16.6349(4)
b / Å	25.9091(5)
c / Å	17.1255(4)
α / °	90
β / °	109.381(3)
γ / °	90
Volume / Å^3	6962.7(3)
Z	4
ρ_{calc} g/cm^3	1.534
μ / mm^{-1}	0.349
F(000)	3264.0
Crystal size / mm^3	0.19 × 0.18 × 0.07
Radiation	Mo Kα (λ = 0.71073)
2Θ range for data collection / °	5.094 to 67.754
Index ranges	$-25 \leq h \leq 21$, $-37 \leq k \leq 40$, $-26 \leq l \leq 23$
Reflections collected	105290
Independent reflections	25143 [Rint = 0.0477, Rsigma = 0.0513]
Data/restraints/parameters	25143/0/1090
Goodness-of-fit on F^2	1.018
Final R indexes [$I \geqq 2\sigma$ (I)]	R_1 = 0.1027, wR_2 = 0.2427
Final R indexes [all data]	R_1 = 0.1383, wR_2 = 0.2670
Largest diff. peak/hole / e Å^{-3}	2.10/-1.43

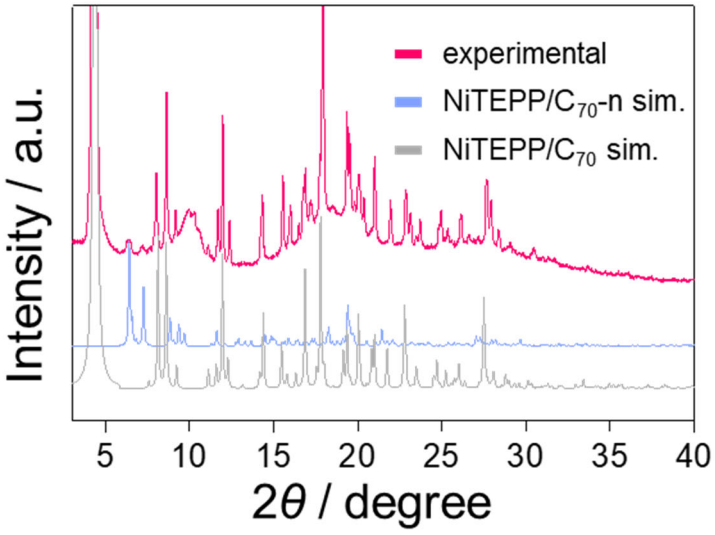

Fig. S12 Experimental PXRD pattern of the bulk sample prepared by Fig. S1, and simulated ones from the **NiTEPP/C$_{70}$-n** and **NiTEPP/C$_{70}$** single crystal structures.

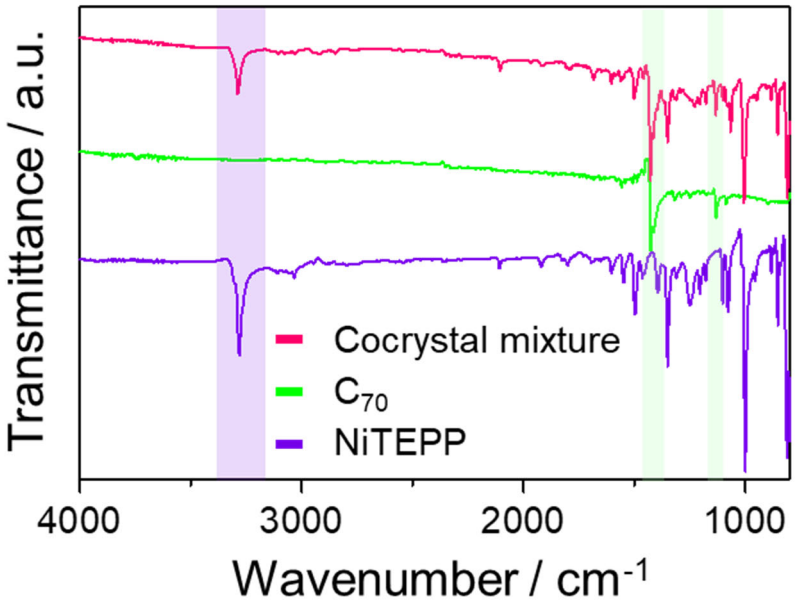

Fig. S13. IR spectra of cocrystal mixture (magenta), C_{70} (green), NiTEPP (purple).

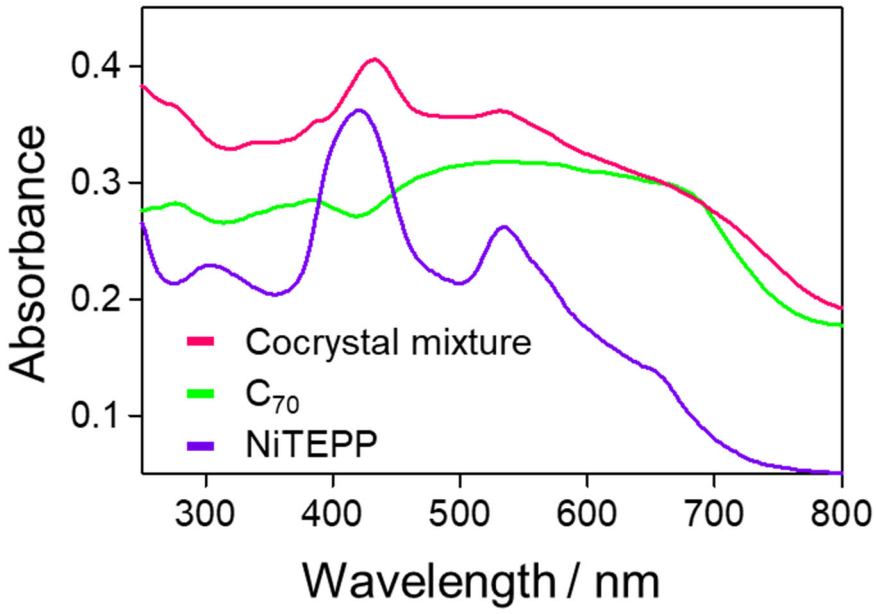

Fig. S14 Solid-state UV/vis absorption spectra of cocrystal mixture (magenta), C_{70} (green), NiTEPP (purple).

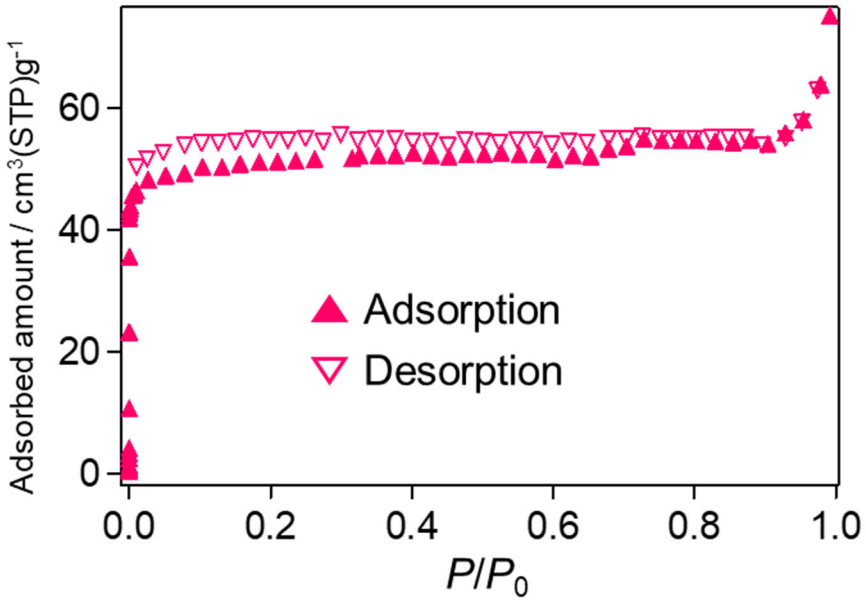

Fig. S15. Nitrogen adsorption/desorption isotherms of cocrystal mixture at 77 K.

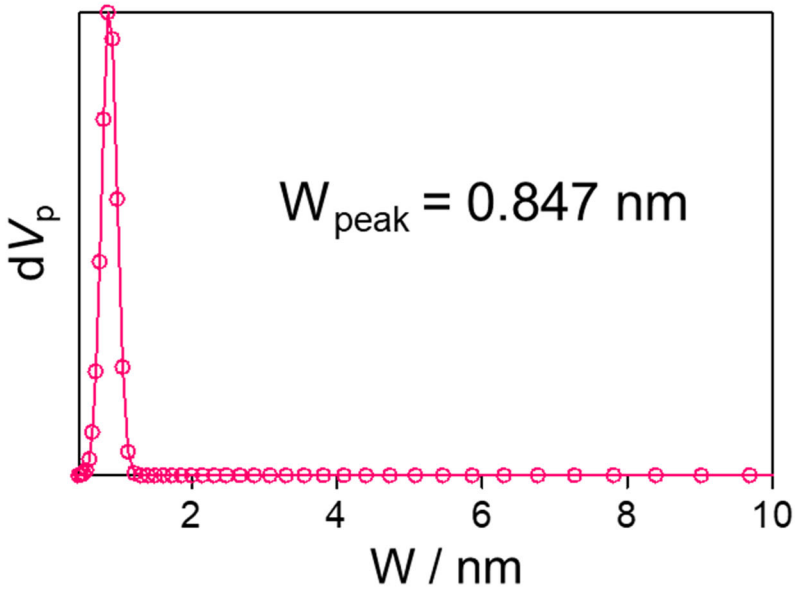

Fig. S16. Pore size distribution data obtained from the nitrogen adsorption isotherm of cocrystal mixture using the NLDFT-GCMC method.

Table S4. Cell parameters of **NiTEPP/C_{70}** obtained from scXRD measurements under applied pressures

Pressure (GPa)	*a* (Å)	*b* (Å)	*c* (Å)	*α* (degree)	*β* (degree)	*γ* (degree)	*V* (Å^3)	Rate of match to detected cell (%)
0	23.67	23.66	21.58	90.01	90.00	120.0	10466	95.25
0.06	23.58	23.60	21.50	90.01	90.03	119.5	10406	70.33
0.32	23.36	23.28	21.26	90.04	90.07	119.4	10075	72.57
0.60	23.037	23.113	21.116	90.04	89.97	119.59	9777	81.54
1.35	23.3565	23.069	20.069	90.3456	89.4408	121.3411	9603.18	7.69
1.92	24.0022	23.6402	20.6182	92.4838	83.7445	130.5201	8834.6038	6.25

Table S5. Cell parameters of **NiTEPP/C_{70}-n** obtained from scXRD measurements under applied pressure

Pressure (GPa)	*a* (Å)	*b* (Å)	*c* (Å)	*α* (degree)	*β* (degree)	*γ* (degree)	*V* (Å^3)	Ratio of match to detected cell (%)
0	16.628	26.9152	16.8575	89.999	107.824	89.981	7182.6	84.55
0.07	16.6292	26.9032	16.856	89.992	107.838	90.001	7179	96.47
0.60	16.67	24.95	16.76	89.99	108.42	90.01	6604	92.8
1.50	16.44	24.59	16.53	89.71	108.9	89.75	6324	87.64
2.17	16.81	25.57	16.76	89.76	113.78	89.68	6592	50.71
3.60	16.51	24.89	16.69	89.82	110.9	90.1	6408	61.48
5.70	16.41	25.25	17.7	90.9	111	90.6	6828	17.14

References for SI

(1) CrysAlisPRO, Oxford Diffraction /Agilent Technologies UK Ltd, Yarnton, England.

(2) VandeVondele, J.; Krack, M.; Mohamed, F.; Parrinello, M.; Chassaing, T.; Hutter, J. Quickstep: Fast and Accurate Density Functional Calculations Using a Mixed Gaussian and Plane Waves Approach. *Comput. Phys. Commun.* **2005**, *167* (2), 103–128. https://doi.org/10.1016/j.cpc.2004.12.014.

(3) Kühne, T. D.; Iannuzzi, M.; Del Ben, M.; Rybkin, V. V.; Seewald, P.; Stein, F.; Laino, T.; Khaliullin, R. Z.; Schütt, O.; Schiffmann, F.; Golze, D.; Wilhelm, J.; Chulkov, S.; Bani-Hashemian, M. H.; Weber, V.; Borštnik, U.; Taillefumier, M.; Jakobovits, A. S.; Lazzaro, A.; Pabst, H.; Müller, T.; Schade, R.; Guidon, M.; Andermatt, S.; Holmberg, N.; Schenter, G. K.; Hehn, A.; Bussy, A.; Belleflamme, F.; Tabacchi, G.; Glöß, A.; Lass, M.; Bethune, I.; Mundy, C. J.; Plessl, C.; Watkins, M.; VandeVondele, J.; Krack, M.; Hutter, J. CP2K: An Electronic Structure and Molecular Dynamics Software Package - Quickstep: Efficient and Accurate Electronic Structure Calculations. *J. Chem. Phys.* **2020**, *152* (19). https://doi.org/10.1063/5.0007045.

(4) Perdew, J. P.; Burke, K.; Ernzerhof, M. Generalized Gradient Approximation Made Simple. *Phys. Rev. Lett.* **1996**, *77* (18), 3865–3868. https://doi.org/10.1103/PhysRevLett.77.3865.

(5) VandeVondele, J.; Hutter, J. Gaussian Basis Sets for Accurate Calculations on Molecular Systems in Gas and Condensed Phases. *J. Chem. Phys.* **2007**, *127* (11), 114105. https://doi.org/10.1063/1.2770708.

(6) Hartwigsen, C.; Goedecker, S.; Hutter, J. Relativistic Separable Dual-Space Gaussian Pseudopotentials from H to Rn. *Phys. Rev. B* **1998**, *58* (7), 3641–3662. https://doi.org/10.1103/PhysRevB.58.3641.

(7) Huang, C.; Pavone, M.; Carter, E. A. Quantum Mechanical Embedding Theory Based on a Unique Embedding Potential. *J. Chem. Phys.* **2011**, *134* (15), 154110. https://doi.org/10.1063/1.3577516.

(8) Makiura, R.; Usui, R.; Sakai, Y.; Nomoto, A.; Ogawa, A.; Sakata, O.; Fujiwara, A. Towards Rational Modulation of In-Plane Molecular Arrangements in Metal–Organic Framework Nanosheets. *ChemPlusChem* **2014**, *79* (9), 1352–1360. https://doi.org/10.1002/cplu.201402150.

(9) Vonhoeren, B.; Dalgleish, S.; Hu, L.; Matsushita, M. M.; Awaga, K.; Ravoo, B. J. Photocurrent Generation in Organic Photodetectors with Tailor-Made Active Layers Fabricated by Layer-by-Layer Deposition. *ACS Appl. Mater. Interfaces* **2015**, *7* (13), 7049–7053. https://doi.org/10.1021/am509031u.

(10) Wang, Z.; Yuan, S.; Mason, A.; Reprogle, B.; Liu, D.-J.; Yu, L. Nanoporous Porphyrin Polymers for Gas Storage and Separation. *Macromolecules* **2012**, *45* (18), 7413–7419. https://doi.org/10.1021/ma301426e.

(11) Bondi, A. Van Der Waals Volumes and Radii. *J. Phys. Chem.* **1964**, *68* (3), 441–451.

https://doi.org/10.1021/j100785a001.